


# Efficient Optimization of Natural Resonance Theory Weightings and Bond Orders by Gram-Based Convex Programming

Eric D. Glendening,<sup>[a]</sup> Stephen J. Wright,<sup>[b]</sup> and Frank Weinhold <sup>\*,[c]</sup>

We describe the formal algorithm and numerical applications of a novel convex quadratic programming (QP) strategy for performing the variational minimization that underlies natural resonance theory (NRT). The QP algorithm vastly improves the numerical efficiency, thoroughness, and accuracy of variational NRT description, which now allows uniform treatment of *all* reference structures at the high level of detail previously reserved only for leading “reference” structures, with little or no user guidance. We illustrate overall QPNRT search strategy, program

I/O, and numerical results for a specific application to adenine, and we summarize more extended results for a data set of 338 species from throughout the organic, bioorganic, and inorganic domain. The improved QP-based implementation of NRT is a principal feature of the newly released *NBO 7.0* program version. © 2019 Wiley Periodicals, Inc.

DOI: 10.1002/jcc.25855

## Introduction

Natural resonance theory (NRT)<sup>[1]</sup> is a widely used method<sup>[2]</sup> for extracting chemically intuitive resonance-type descriptors from the first-order reduced density matrix (1-RDM,  $\Gamma$ )<sup>[3]</sup> of quantum chemical theory. As originally recognized by Kekulé, Robinson, Lowry, Ingold, and others,<sup>[4]</sup> and subsequently formulated in quantum mechanical terms by Pauling,<sup>[5]</sup> chemical species cannot generally be described by a single Lewis-structural bonding pattern, but must instead be conceived as a “resonance hybrid” (chemical superposition<sup>[6]</sup>) of alternative bonding patterns  $\text{I} \leftrightarrow \text{II} \leftrightarrow \text{III} \leftrightarrow \dots$  with associated probability weights  $w_{\text{I}}, w_{\text{II}}, w_{\text{III}}, \dots$ . Such resonance-type conceptions and associated curly-arrow, electron-pushing mnemonics are now ubiquitous features of chemical pedagogy and practice throughout the molecular sciences. While earlier applications of resonance theory were largely empirical in character,<sup>[7]</sup> such conceptions can now be rigorously supported by variational NRT algorithms<sup>[1]</sup> that allow chemically intuitive resonance weights and bond-order descriptors to be derived from virtually any high-level quantum chemical method in current usage.<sup>[8]</sup>

A mathematical outline of NRT algorithms can be sketched as follows [employing a common notation to distinguish operator/matrix (bold upper case), vector (bold lower case), and set-theoretic (parentheses or bold script) quantities]. The full quantum-chemical 1-RDM  $\Gamma_{\text{QC}}$  of the system is variationally approximated as a probability-weighted sum ( $\Gamma_{\text{NRT}}$ ) of contributions  $\Gamma_{\text{I}}, \Gamma_{\text{II}}, \Gamma_{\text{III}}, \dots$  from individual localized resonance structures

$$\mathbf{\Gamma}_{\text{NRT}} = w_{\text{I}}\mathbf{\Gamma}_{\text{I}} + w_{\text{II}}\mathbf{\Gamma}_{\text{II}} + w_{\text{III}}\mathbf{\Gamma}_{\text{III}} + \dots \quad (1a)$$

with nonnegative weights  $\{w_R\}$  that sum to unity

$$w_{\text{I}} + w_{\text{II}} + w_{\text{III}} + \dots = 1, \text{ all } w_R \geq 0 \quad (1b)$$

The weights are variationally optimized, subject to eq. (1b), to minimize the NRT objective function  $\Delta(\{w_R\})$ , which can be described as the root-mean-square deviation of  $\mathbf{\Gamma}_{\text{NRT}}$  from the actual quantum-chemical 1-RDM  $\mathbf{\Gamma}_{\text{QC}}$  (expressed more precisely in Frobenius matrix norm notation in equations to follow). Each matrix  $\mathbf{\Gamma}_{\text{QC}}$  and  $\mathbf{\Gamma}_{\text{NRT}}$  is of dimension  $n_b$  (the number of basis functions) and serves to describe the alpha (spin-up) or beta (spin-down) electron distribution of the quantum-chemical system, allowing for different values of the objective function (and different resonance weightings, etc.) for different spins of an open-shell system. Of course, for spin-restricted treatments, the alpha and beta weights are identical.

Quantum-chemical evaluation of any one-electron property  $\langle \mathbf{P}_{1e} \rangle_{\text{QC}}$  requires only a simple convolution of operator  $\mathbf{P}_{1e}$  and  $\mathbf{\Gamma}_{\text{QC}}$ , written symbolically as the integrated product of  $\mathbf{P}_{1e}(\mathbf{r})$  with the kernel  $\mathbf{\Gamma}(\mathbf{r}|\mathbf{r}')$  of  $\mathbf{\Gamma}_{\text{QC}}$  over all one-electron coordinate and spin space  $\mathbf{r}$ ,<sup>[3]</sup>

[a] E. D. Glendening  
Department of Chemistry and Physics, Indiana State University, Terre Haute, Indiana 47809  
E-mail: eric.glendening@indstate.edu

[b] S. J. Wright  
Department of Computer Science, University of Wisconsin–Madison, Madison, Wisconsin 53705  
E-mail: swright@cs.wisc.edu

[c] F. Weinhold  
Theoretical Chemistry Institute and Department of Chemistry, University of Wisconsin–Madison, Madison, Wisconsin 53705  
E-mail: weinhold@chem.wisc.edu

Contract Grant sponsor: National Science Foundation; Contract Grant number: CHE-0840494

© 2019 Wiley Periodicals, Inc.

$$\langle \mathbf{P}_{1e} \rangle = \int [\mathbf{P}_{1e}(\mathbf{r}) \Gamma(\mathbf{r}|\mathbf{r}')]_{\mathbf{r}' \rightarrow \mathbf{r}} d\mathbf{r} \quad (2)$$

The mathematical structure of the NRT ansatz (1a) then guarantees that any calculable one-electron property (such as dipole moment, kinetic energy, nuclear-electron attraction, molecular geometry,<sup>[9]</sup> or any property that depends solely on electron density) will optimally satisfy

$$\langle \mathbf{P}_{1e} \rangle_{\text{QC}} \approx w_I \langle \mathbf{P}_{1e} \rangle_I + w_{II} \langle \mathbf{P}_{1e} \rangle_{II} + w_{III} \langle \mathbf{P}_{1e} \rangle_{III} + \dots \quad (3)$$

Relationship (3) ensures optimal consistency with the fundamental resonance-theoretic assumption that properties of the resonance hybrid species are expressible as the probability-weighted average of corresponding properties for individual resonance structures. In contrast to the  $\Gamma$ -based expression (2) for evaluation of chemical properties, a Pauling-type (wavefunction-based) formulation of the resonance Ansatz cannot satisfy the original “averaging” concept that underlies mesomerism theory.

Because eqs. (1a) and (1b) are nonlinear, previous numerical implementation of the NRT search in the natural bond orbital (NBO) program, *NBO 6.0*,<sup>[10]</sup> offered a variety of gradient-based nonlinear minimization methods, including conjugate gradient, Broyden–Fletcher–Goldfarb–Shanno, and simulated annealing algorithms.<sup>[11]</sup> These methods do not exploit a key property of the formulation—the fact that it is a convex quadratic program (QP). Convexity is a property of optimization problems that ensures all local solutions are global solutions, and that bounds can be found on the amount of computational effort required to identify such a solution (to within a prescribed tolerance). The problem is a quadratic program, because the objective function for expansion (1a) is a quadratic function of the variables, and the constraints (1b) are linear equalities and inequalities. In fact, the inequality constraints in this problem define a *simplex* (all variables are nonnegative and sum to unity) common structure that can be handled efficiently by algorithms.

We describe in this paper an active-set QP approach for solving eqs. (1a) and (1b). Other methods for convex QP could be applied (including a primal-dual interior-point method and a gradient projection method) but the active-set approach described here is efficient in practice and it exploits fully the properties of the problem. It is able to solve much larger problems than the general nonlinear optimization methods implemented for legacy NRT in *NBO 6.0*, and is now fully implemented in current *NBO 7.0*.<sup>[12]</sup>

## Gram–Lagrangian minimization of the NRT objective function

Let us suppose that  $n_R$  is the number of resonance structures in the representation of  $\Gamma_{\text{NRT}}$ . The unknowns  $w_I, w_{II}, w_{III}, \dots$  in eqs. (1a) and (1b) can be gathered into a vector  $\mathbf{w} \in \mathbb{R}^{n_R}$ , the real space of dimension  $n_R$ . The constraints (1b) can be written as

$$\sum_{R=1}^{n_R} w_R = \mathbf{e}^T \mathbf{w} = 1, \mathbf{w} \geq 0 \quad (4)$$

where superscript “ $T$ ” denotes transposition,  $\mathbf{e} = (1, 1, \dots, 1)^T$ , and the notation  $\mathbf{w} \geq 0$  signifies that all components of vector

$\mathbf{w}$  are nonnegative. The objective function to be minimized is the matrix root-mean-square deviation

$$\Delta(\{\mathbf{w}_R\}) = \min_{\{\mathbf{w}_R\}} \sqrt{\frac{\|\Gamma_{\text{QC}} - \Gamma_{\text{NRT}}\|_F^2}{n_b}} \quad (5)$$

By the definition of the Frobenius norm, we can rewrite this objective as

$$\Delta(\{\mathbf{w}_R\}) = \sqrt{\frac{\mathbf{w}^T \mathbf{G} \mathbf{w}}{n_b}} \quad (6)$$

where  $\mathbf{G}$  is the Gram matrix of elements

$$G_{R,R'} = \text{Trace} \left( (\Gamma_{\text{QC}} - \Gamma_R)^T (\Gamma_{\text{QC}} - \Gamma_{R'}) \right), \text{ for } R, R' = 1, 2, \dots, n_R \quad (7)$$

We now describe an active-set strategy for solving the convex QP to minimize  $\Delta(\{\mathbf{w}_R\})$  (or, equivalently, the quadratic function  $\mathbf{w}^T \mathbf{G} \mathbf{w}$ ). The technique follows Algorithm 16.3 of Ref. [13], adapted to the particular QP encountered here, with additional details about the linear algebra calculations required at each step.

The condition for an optimal solution point  $\mathbf{w}^*$  of the minimization problem (6) subject to the constraints (4) is that there exists an *active set*  $\mathcal{W}^* \subset \{1, 2, \dots, n_R\}$  such that

$$\mathbf{G} \mathbf{w}^* + \lambda^* \mathbf{e} - \sum_{R \in \mathcal{W}^*} \mu_R^* \mathbf{e}_R = 0 \quad (8a)$$

$$\mathbf{e}^T \mathbf{w}^* = 1 \quad (8b)$$

$$\mathbf{w}_R^* = 0 \text{ for all } R \in \mathcal{W}^* \quad (8c)$$

$$\mu_R^* \geq 0 \text{ for all } R \in \mathcal{W}^* \quad (8d)$$

$$\mathbf{w}_R^* \geq 0 \text{ for all } R \in \{1, 2, \dots, n_R\} \setminus \mathcal{W}^* \quad (8e)$$

The Lagrange parameters  $\lambda^*$  and  $\mu_R^*$  (for  $R \in \mathcal{W}^*$ ) are real numbers and  $\mathbf{e}_R$  is the vector in  $\mathbb{R}^{n_R}$  that contains all zeros except for a 1 in position  $R$ . A more compact form of (8) is obtained by defining the matrix  $\mathbf{E}_{\mathcal{W}^*}$  and vector  $\mu_{\mathcal{W}^*}$  as follows

$$\mathbf{E}_{\mathcal{W}^*} := [\mathbf{e}_R]_{R \in \mathcal{W}^*} \quad (9a)$$

$$\mu_{\mathcal{W}^*} := [\mu_R]_{R \in \mathcal{W}^*}^T \quad (9b)$$

Equations (8a)–(8e) are then written equivalently as

$$\mathbf{G} \mathbf{w}^* + \lambda^* \mathbf{e} - \mathbf{E}_{\mathcal{W}^*} \mu_{\mathcal{W}^*}^* = 0 \quad (10a)$$

$$\mathbf{e}^T \mathbf{w}^* = 1 \quad (10b)$$

$$\mathbf{E}_{\mathcal{W}^*}^T \mathbf{w}^* = 0 \quad (10c)$$

$$\mu_{\mathcal{W}^*}^* \geq 0 \quad (10d)$$

$$\mathbf{w}^* \geq 0 \quad (10e)$$

The obvious approach of finding  $\mathcal{W}^*$  by trying all  $2^{n_R}$  possible choices and selecting the one for which  $\mathbf{w}^*$ ,  $\lambda^*$ , and  $\mu^*$

satisfying (10) is computationally intractable for any  $n_R$  of reasonable size. The active-set method proceeds by making a sequence of guesses of  $\mathcal{W}^*$ , changing only one component at each iteration, working systematically, iteration by iteration, toward the optimal value  $\mathcal{W}^*$ . At iteration  $k$ , the active-set method also produces an estimate  $\mathbf{w}^k$  of the solution  $\mathbf{w}^*$ , where  $\mathbf{w}^k$  satisfies the constraints (4), along with estimates  $\mu^k$  and  $\lambda^k$  of  $\mu^*$  and  $\lambda^*$  in (10), respectively. Each iterative step involves determination of a “projected step”  $\mathbf{p}^k$ , obtained from solution of a system of simultaneous linear eq. (11),

$$\begin{pmatrix} \mathbf{G} & \mathbf{e} & -\mathbf{E}_{\mathcal{W}^k} \\ \mathbf{e}^T & 0 & 0 \\ \mathbf{E}_{\mathcal{W}^k}^T & 0 & 0 \end{pmatrix} \begin{pmatrix} \mathbf{p}^k \\ \lambda^k \\ \mu_{\mathcal{W}^k}^k \end{pmatrix} = \begin{pmatrix} -\mathbf{G}\mathbf{w}^k \\ 0 \\ -\mathbf{E}_{\mathcal{W}^k}\mathbf{w}^k \end{pmatrix}. \quad (11)$$

A positive multiple of  $\mathbf{p}^k$  can be added to current  $\mathbf{w}^k$  to obtain the next estimate  $\mathbf{w}^{k+1}$ . An adjustment to the working set  $\mathcal{W}^k$  is usually made too. We outline the active-set algorithm for the QPNRT solver in Figure 1, using set-theoretic notation.<sup>[13]</sup> The main steps are as follows. Iteration  $k$  starts by solving eq. (11), which is formed from the first three equality conditions in (10), for the current values of Lagrange multipliers  $\lambda^k$  and  $\mu_{\mathcal{W}^k}^k$ . If  $\mathbf{p}^k = 0$  and  $\mu_{\mathcal{W}^k}^k \geq 0$ , then we have found the solution: We can set  $\mathcal{W}^* = \mathcal{W}^k$ ,  $\mathbf{w}^* = \mathbf{w}^k$ ,  $\lambda^* = \lambda^k$ , and  $\mu_{\mathcal{W}^*}^* = \mu_{\mathcal{W}^k}^k$ , and terminate. Otherwise, if  $\mathbf{p}^k = 0$  but the components of  $\mu_{\mathcal{W}^k}^k$  are not all non-negative, we choose some  $j \in \mathcal{W}^k$  for which  $\mu_j^k < 0$ , and drop index  $j$  from the set  $\mathcal{W}^k$  in preparation for the next iteration.

Otherwise, if  $\mathbf{p}^k \neq 0$ , we take a step from  $\mathbf{w}^k$  in the direction  $\mathbf{p}^k$  stopping as soon as one of the bounds  $\mathbf{w}_j \geq 0$  is about to be violated, or at a step length of 1, whichever comes first. If a bound  $\mathbf{w}_j \geq 0$  is encountered, we add  $j$  to the set  $\mathcal{W}^k$  in preparation for the next iteration. Otherwise, we leave  $\mathcal{W}^k$  unchanged, setting  $\mathcal{W}^{k+1} = \mathcal{W}^k$  and proceeding to the next iteration.

We often encounter a situation in which eq. (6) has multiple solutions, that is, there is more than one vector  $\mathbf{w}^*$  (with some  $\mathcal{W}^*$ ,  $\lambda^*$ , and  $\mu^*$ ) that satisfy (10). This situation, known as a type of degeneracy, can arise when the Gram matrix (7) is positive semidefinite (that is, it has zero eigenvalues as well as strictly positive eigenvalues). When multiple solutions exist, they are all equally valid from an optimization viewpoint. However, from the viewpoint of the application, we favor NRT solutions in which the nonzero components of  $\mathbf{w}^*$  for symmetry-equivalent resonance forms take the same value. We have found that regularizing the Gram matrix, by replacing  $\mathbf{G}$  by  $\mathbf{G} + \delta \mathbf{I}$  in eq. (11) (where  $\delta = 1.0 \times 10^{-3}$ ), generates solutions of this type. Regularization has the effect of adding a term  $\delta \|\mathbf{w}\|^2$  to the objective function  $\mathbf{w}^T \mathbf{G} \mathbf{w}$  that steers the optimization algorithm to the element in the solution set with minimal Euclidean norm, which is usually the one in which the nonzero components have the same value.

## Integrated strategy for resonance structure selection and resonance weight optimization

The two principal tasks for NRT analysis are generating candidate resonance structures and optimizing the resonance

weights. The latter is sufficiently efficient with the QP solver that we have been able to implement an iterative strategy for generating and selecting resonance structures that can be applied to systems that were essentially impossible to treat with legacy NRT in *NBO 6.0*. We now describe this new strategy, as implemented in *NBO 7.0*, and show its application in NRT analysis of the adenine molecule. A schematic overview of the overall strategy is shown in Figure 2.

NRT begins by acquiring an initial set of candidate structures from three sources, including (1) the natural Lewis structure (NLS) of the NBO search, (2) a search for plausible bonding patterns in the natural bond index values, and (3) user-supplied structures provided by \$NRTSTR keylist input (if present). Each candidate structure is stored in “TOPO matrix form,” that is, in an  $n_a \times n_a$  integer array, where  $n_a$  is the number of atoms, with diagonal elements equal to the number of lone pairs on the respective atoms and off-diagonal elements equal to the bond orders for atom pairs.

The resulting set of TOPO matrices guide NBO’s CHOOSE algorithm as it searches  $\Gamma_{\text{QC}}$  for the set of bonds and lone pairs that optimally describe the electron density  $\Gamma_R$  of each resonance structure. The atomic hybrids that comprise the bonds and lone pairs are obtained from the eigenvectors of one- and two-center blocks of  $\Gamma_{\text{QC}}$ , rather than from frozen hybrids of a parent resonance form as used for some structures in the original NRT implementation. Thus, the resonance structures in our new NRT strategy are generally better in representing the electron density of the associated bonding pattern than the structures of the legacy NRT approach. Note that the CHOOSE-optimized NBOs generally differ from one  $\Gamma_R$  bonding pattern to another, so no assumptions are made concerning orthogonality of contributing resonance structures.

The CHOOSE algorithm allows single TOPO matrices to yield multiple resonance forms, as is the case, for example, with the doubly-bonded resonance structures of  $\text{CO}_2$ . The  $\text{O}=\text{C}=\text{O}$  bonding pattern can be represented by a single TOPO matrix but corresponds to two resonance structures, one with a  $\pi_x$  bond on the left and a  $\pi_y$  on the right, and another with  $\pi_y$  on the left and  $\pi_x$  on the right. CHOOSE detects alternative bonding options in its search of  $\Gamma_{\text{QC}}$  and generates multiple resonance forms from single TOPO matrices when appropriate.

Given the set of densities  $\{\Gamma_R\}$ , NRT constructs the regularized Gram matrix of eq. (7) and proceeds to minimize the resonance weights. Given no other information, the QP solver assigns all resonance structures to the active set except the single structure that best represents  $\Gamma_{\text{QC}}$ . That is, the solver begins with a resonance expansion (1a) consisting of just one structure ( $w_1^0 = 1$ ) with all other structures assigned to the active set ( $\mathcal{W}^0$  of Fig. 1). The solver then proceeds to iteratively evaluate eq. (11), following the algorithm of Figure 1, moving one structure at a time from the active set to the resonance expansion, or vice versa, until the solution to eq. (11) satisfies eq. (10a)–(10e). The result is the optimal resonance expansion (1a) subject to the constraints (1b). If the QP solver has information about a prior minimization for  $\Gamma_{\text{QC}}$ , the solver instead begins with the resonance expansion of the earlier minimization, adjusts the active set accordingly, and proceeds to solve eq. (11).

Choose initial  $\mathbf{w}^0$  satisfying (4) and  $\mathbf{w}^0 \subset \{i | w_i^0 = 0\}$ ;

for  $k = 0, 1, 2, \dots$  do

Solve for  $\mathbf{p}^k$ :

$$\begin{pmatrix} \mathbf{G} & \mathbf{e} & -\mathbf{E}\mathbf{w}^k \\ \mathbf{e}^T & \mathbf{0} & \mathbf{0} \\ \mathbf{E}^T\mathbf{w}^k & \mathbf{0} & \mathbf{0} \end{pmatrix} \begin{pmatrix} \mathbf{p}^k \\ \lambda^k \\ \boldsymbol{\mu}_{\mathbf{w}^k}^k \end{pmatrix} = \begin{pmatrix} -\mathbf{G}\mathbf{w}^k \\ 0 \\ -\mathbf{E}\mathbf{w}^k\mathbf{w}^k \end{pmatrix};$$

if  $\mathbf{p}^k = \mathbf{0}$  then

if  $\boldsymbol{\mu}_{\mathbf{w}^k}^k \geq \mathbf{0}$  then

STOP with solution  $\mathbf{w}^* = \mathbf{w}^k$  and optimal active set  $\mathbf{w}^* = \mathbf{w}^k$ ;

else

Choose  $j \in \mathbf{w}^k$  with  $\mu_j^k < 0$ ;

Set  $\mathbf{w}^{k+1} \leftarrow \mathbf{w}^k$  and  $\mathbf{w}^{k+1} \leftarrow \mathbf{w}^k \setminus \{j\}$ ;

end if

else

Choose  $\alpha_k := \min\left(1, \min_{j \in \mathbf{w}^k, p_j^k < 0} \frac{-w_j^k}{p_j^k}\right)$  and set  $\mathbf{w}^{k+1} \leftarrow \mathbf{w}^k + \alpha_k \mathbf{p}^k$ ;

if there is  $j \in \mathbf{w}^k$  such that  $w_j^k > 0$  and  $w_j^{k+1} = 0$  then

Add one such  $j$  to  $\mathbf{w}^k$  to obtain  $\mathbf{w}^{k+1}$ ;

else

Set  $\mathbf{w}^{k+1} \leftarrow \mathbf{w}^k$ ;

end if

end if

end for

Figure 1. The active-set algorithm for solving the convex QP (4), (6) for NRT weights.

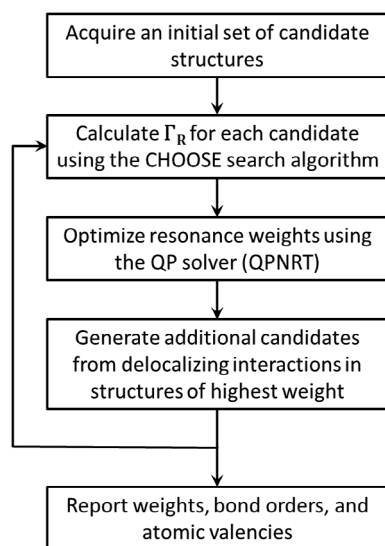


Figure 2. Schematic overview of integrated NRT solution strategy (with QPNRT solver for resonance weightings as middle box).

With an optimized resonance expansion in hand, NRT must now decide whether to augment the set of candidate structures or terminate its search. NRT identifies a set of leading resonance structures in the expansion and uses each of these

structures in turn as a “parent” structure for generating additional “daughter” bonding patterns. For each parent structure, NRT performs second-order perturbative analysis of the NBO Fock or Kohn–Sham matrix (or a closely related approximation involving density matrix elements for multiconfiguration wavefunctions, as in previous NRT), seeking strong delocalizing interactions among the valence NBOs. These interactions correspond to bond rearrangements, as shown in Figure 3, and have the potential to generate new bonding patterns that were not previously considered by NRT. If, after considering all reference structures, no new patterns emerge, NRT terminates, reporting the resonance expansion, bond orders, and atomic valencies. Otherwise, NRT cycles back to the CHOOSE step, calculating new resonance structures and repeating QP minimization. Note that these interleaved recursive strategies involve the successive “cycles” of resonance structure additions (each summarized in a line of NRT output) and the QP “iterations” (with only  $k_{\max}$  values listed for each cycle).

Controlling the search for additional resonance forms will be a primary concern for the NRT user. The search is directed by two thresholds that we refer to here by their user-selectable keywords (NRTPAR and NRTE2 of the \$NBO keylist program input). NRTPAR sets the threshold determining whether a structure in the resonance expansion will be treated as a parent for

NBO	parent NLS	CT resonance
amide $n_N \rightarrow \pi^*_{CO}$		$N^+ = C - \ddot{O}^-$
vicinal $\pi_{CC} \rightarrow \pi^*_{CC}$		$C^+ - C = C - C^-$
vicinal $\sigma_{AX} \rightarrow \sigma^*_{BY}$		$X^+ \quad A = B \quad Y^-$
geminal $\sigma_{AX} \rightarrow \sigma^*_{AY}$		$X^+ \quad Y^- \quad A:$
H-bond $n_B \rightarrow \sigma^*_{AH}$		$B^+ - H \quad A^-$

**Figure 3.** General mapping of NBO donor-acceptor types (left) onto associated curly-arrow representation (center) and resultant charge transfer resonance structure depiction (right) for a variety of bonding motifs.

potential daughter structures or not. By default, NRTPAR = 50%, which sets the parent threshold to 50% of the weight for the leading structure in the expansion. For example, if the weight of the leading structure is 0.30, all structures in the expansion

having weights greater than 0.15 (i.e., 50% of 0.30) will be treated as parents in the search for new daughter structures. NRTE2 sets the threshold for judging whether delocalizing interactions in a parent structure are sufficiently strong to generate one or more new bonding patterns to be considered (by the QP solver) for inclusion in the resonance expansion. By default, NRTE2 = 1, meaning that all delocalizations stronger than 1 kcal/mol have the potential to generate new patterns. Note that in contrast to the original NRT version, *all* NRT resonance structures are now treated with full “reference structure” detail, using the improved CHOOSE search that is essentially similar to the fully optimized NLS search of default NBO analysis. Note also that decreasing either NRTPAR or NRTE2 adds to the costly overhead of CHOOSE optimizations for an increasing proliferation of resonance structures that are unlikely to significantly improve the QP solution.

Figure 4 shows sample output for a relatively unconstrained QPNRT description of adenine at the B3LYP/6-311++G\*\* level. The NRT output begins by reporting the NRTPAR and NRTE2 thresholds, which are the default 50% and 1 kcal/mol values, respectively, for this calculation. NRT then acquires two initial bonding patterns (TOPO matrices), one from the NLS of the NBO search and one from the search of the natural binding index connectivity pattern. NRT detects molecular point group symmetry (from evident symmetries of the density matrix) and, unless disabled, augments the list of candidate resonance forms by any missing symmetry equivalent structures. For this adenine calculation, the symmetry routines do not detect any missing structures, and no limit was set (using the NRTCYC = 0 keyword) on the number of iterative cycles that might be required to complete the QPNRT search.

NRT proceeds to optimize the adenine resonance expansion in 11 cycles, where each cycle consists of CHOOSE searches for densities  $\Gamma_R$ , QP minimization of weights for the current list of candidate structures, and generation of additional bonding patterns to be considered in the next cycle. For example, NRT begins the first cycle with two TOPO matrices for which three

#### NATURAL RESONANCE THEORY ANALYSIS:

Parent structure threshold: 50% of leading weight  
Delocalization list threshold: 1 kcal/mol  
Maximum search cycles: unlimited

Cs symmetry, 2 symmetry operator(s), 1 unique atom permutation(s)  
2 initial TOPO matrices: NLS = 1; NBI = 1; SYM = 0

cycle	structures	D(w)	kmax	CHOOSE	ION	E2	SYM	dbmax	dbrms
1	2/2	0.07648873	2	3	0	123	0	2.000	1.287
2	30/96	0.06964206	35	294	0	353	0	0.351	0.149
3	84/354	0.06806869	92	2124	-31	165	0	0.161	0.057
4	99/468	0.06803433	70	1121	-24	569	0	0.020	0.007
5	109/1039	0.06782941	101	6886	-168	136	0	0.041	0.019
6	93/1131	0.06765337	60	702	-24	64	0	0.078	0.020
7	99/1131	0.06760805	26	805	-49	79	0	0.022	0.006
8	87/1189	0.06751115	37	603	-2	122	0	0.039	0.014
9	84/1288	0.06745947	41	1948	-14	282	0	0.025	0.010
10	90/1454	0.06736926	36	3103	-63	91	0	0.042	0.011
11	87/1460	0.06736118	16	513	-65	0	0	0.015	0.005

QPNRT(87/1460): D(0)=0.09093658; D(w)=0.06736118; dbmax=0.015; dbrms=0.005  
Timing(sec): search=334.37; Gram matrix=124.33; minimize=5.73; other=2.87

**Figure 4.** Sample NRT output showing the iterative convergence of the resonance hybrid, objective function value, and bond orders for adenine.

CHOOSE searches (the “CHOOSE” column) are performed. These searches yield two candidate resonance structures, and QP minimization yields an optimal resonance hybrid consisting of two structures from two candidates (“2/2” in the “structures” column) with an objective function value “D(w)” of 0.07648873. A search for strong delocalizing interactions identifies 123 additional TOPO matrices (the “E2” column) to be considered in the next cycle. In the ninth cycle, the QP solver returns a resonance hybrid consisting of 84 resonance structures from 1288 candidates, with an objective function value of 0.06745947. In the 11th cycle, no new bonding patterns are found for further consideration and the NRT search self-terminates.

Resonance structures can be discarded during the NRT procedure. CHOOSE searches yield optimized polar covalent bonds, so that bond ionicity is intrinsic to the bonds that comprise the resonance structures and there is no need to treat bond ionicity via covalent/ionic resonance mixing. If ionic resonance forms (differing solely from a covalent form by the complete polarization of one bond) are detected, they are discarded (the “ION” column). For example, Figure 4 shows that 31 ionic resonance forms were discarded in the third cycle. Bond-order convergence is reported from cycle to cycle, including the maximum change in a bond order (“dbmax”) from one cycle to the next, and the root-mean-square change (“dbrms”) for bond orders exceeding  $1 \times 10^{-3}$ .

The NRT search concludes with a two-line summary report. “D(0)” is the lowest objective function value for a resonance hybrid consisting of only one resonance structure, equivalent to the minimum diagonal element of the Gram matrix. Comparison of  $D(0)$  with the optimal objective function value  $D(w)$  measures the extent to which the NRT resonance description improves that of a single Lewis structure. Timing information is also reported, showing that the bulk of the calculation time is in the CHOOSE searches and in the construction of the Gram matrix. QP minimization is essentially free in this case. The NRT optimization of adenine resonance hybrid, with over 18,000 CHOOSE searches and multiple QP minimizations with hundreds of candidate resonance structures, requires a little over 7 min to complete on a single Xeon 2.60GHz processor. Figure 5 shows the resulting NRT bond orders from the final 87-term resonance expansion.

The principal results of NRT analysis are the bond-order descriptors ( $b_{AB}$ ) that are expected to exhibit useful correlations with bond lengths,<sup>[14]</sup> bond energies,<sup>[15]</sup> bond frequencies (Badger’s rule),<sup>[16]</sup> and other physical properties. As an example, Figure 6 displays the bond-order-bond-length (BOBL) correlation for the nine CN bonds of adenine (Fig. 4), including the BOBL regression fit (dashed line; Pearson  $|\chi|^2 = 0.87$ ). As shown in the final two columns of NRT output in Fig. 4, the NRT bond orders converge systematically toward well-defined numerical limits (intermediate between standard single-, double-, or triple-bond values of idealized single resonance structures), suggesting their predictive utility even for fine details of observable properties. In contrast, the NRT weightings of individual resonance structures tend to lose any semblance of “dominant” or “parent” character as the complexity of the resonance hybrid increases.

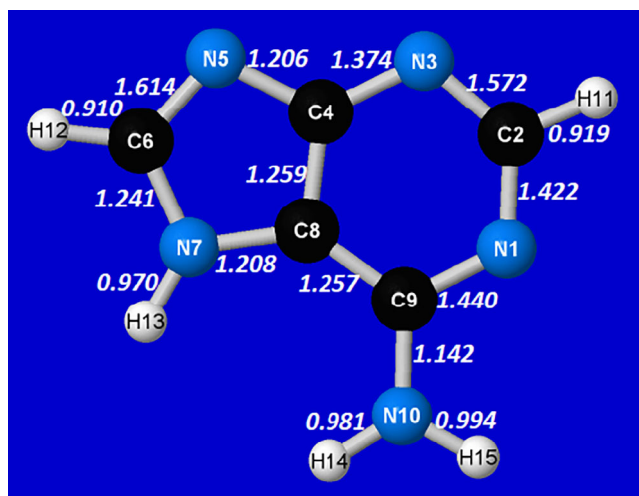
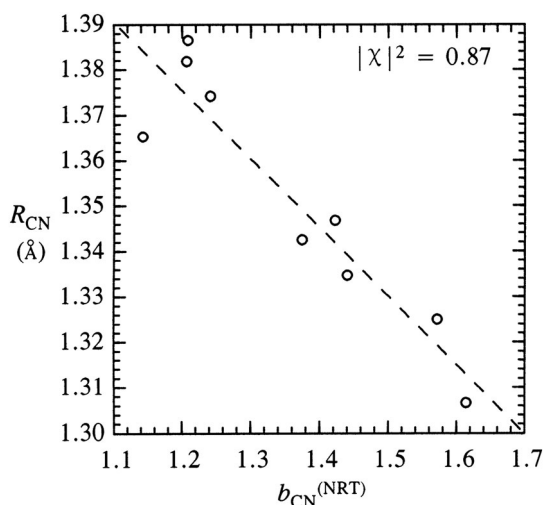


Figure 5. NRT bond orders of adenine (B3LYP/6–311++G\*\* level). [Color figure can be viewed at [wileyonlinelibrary.com](http://wileyonlinelibrary.com)]

## NRT applications to organic, inorganic, and biochemical species

To gain an overview of overall NRT computational performance and set default values for algorithmic keywords affecting performance, we compiled a data set of 338 chemical species of widely varying character and degree of difficulty, chosen (in rather random fashion) as “interesting” examples from the organic, inorganic, and biochemical domain, with sizes ranging up to 108 atoms and 1596 basis functions. The complete list of species and associated NRT performance measures are provided as an *Excel* spreadsheet (Table S1) in Supporting Information. Here, we summarize the results in general statistical terms, mention some noteworthy features of individual species, and explain how current keyword parameters for the default QPNRT search were ultimately selected as a compromise between exhaustive exploration of exotic resonance possibilities and computational practicality.

The form and content of Table S1 evolved as results for variations of certain keyword control parameters became apparent, particularly NRTCYC, NRTPAR, and NRTE2 keywords. The NRTCYC keyword [current default: NRTCYC = 3] sets the maximum allowed number of search cycles for generating additional possible resonance structures to be included in the QPNRT convex solution (which is always allowed to run to convergence), while NRTPAR and NRTE2 (explained above) constrain what structures may be considered as “possible” additional structures for consideration (requiring full CHOOSE optimization) in each new cycle. Any relaxation of these constraints increases the number of candidate resonance structures that must be CHOOSE-optimized (roughly equivalent to a single run of ordinary NBO analysis) and stored. Because the yield of productive structures (i.e., those retained by the convex solver in the optimized description) tends to sharply diminish in later cycles, it is found that system computational times and memory demands tend to become exorbitant as NRTCYC increases, with little appreciable effect on individual bond orders or overall  $D(w)$ . In a large majority of “ordinary” chemical species, the QPNRT



**Figure 6.** NRT BOBL correlation for CN bonds of adenine (cf. Fig. 4), showing least-squares regression fit (dashed line,  $|\chi|^2 = 0.87$ ).

solution achieves full convergence within 1–3 cycles, whereas larger or more troublesome jobs often require more than three cycles and can overrun the maximum allowed number of resonance structures (current default, NRTRES = 10,000), available system resources for the FILE48 read-write file, and/or reasonable time limits, particularly for ligated polynuclear metal clusters or polycyclic organic species beyond the simple adenine example considered above.

Table S1 reports results for the default limit (NRTCYC = 3) of NRT search cycles in *NBO 7.0* as currently distributed, as well as other low NRTCYC values or the unlimited case (requested by NRTCYC = 0) for which the search algorithm runs to self-terminating conclusion. The first sheet summarizes a variety of “averages” for each NRTCYC value, including (e.g., for NRTCYC = 3) the average number of atoms (**natoms** = 27), basis functions (**nbas** = 417), contributing resonance structures (**nres** = 91), and “candidate” resonance structures (**ncand** = 1500). These averages refer to the values listed on

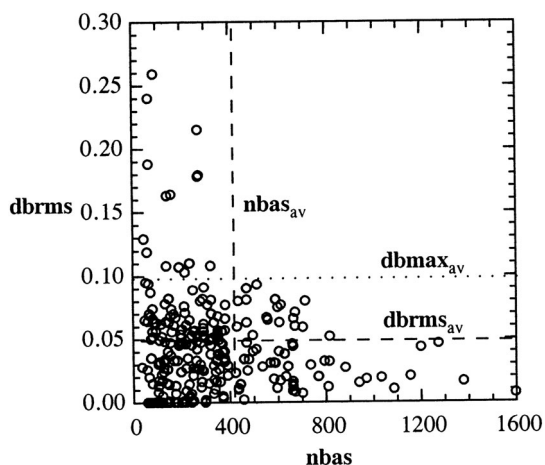


**Figure 7.** Variations in **dbrms** (root-mean-square  $\Delta b_{\text{NRT}}$  corrections in the last cycle of QPNRT search) with **nbas** (number of basis functions) for the 338 species of Table S1. Horizontal lines mark the average values for mean (**dbrms<sub>av</sub>**, dashed) and maximum (**dbmax<sub>av</sub>**, dotted) last-cycle correction, and the dashed vertical line marks average system size (**nbas<sub>av</sub>**) for the data set.

sheet 3 [“NRTCYC = 3 (default)”] with species sizes ranging up to 108 atoms, 1596 basis functions, and up to 20,000 allowed candidate structures. As a qualitative measure of bond-order convergence, the summaries also show the average bond-order change in the final cycle, both for the largest (**dbmax** = 0.09) and root-mean-square change (**dbrms** = 0.04). The final three sheets display comparisons of species for which QPNRT results were obtained for NRTCYC = 3 (202 species), 4 (130 species), or 5 (100 species). For example, “W24” [(H<sub>2</sub>O)<sub>24</sub> water cluster] results could be completed for NRTCYC = 3 or 4, but not for NRTCYC = 5.

Figure 7 portrays some statistical features of the data set for default (NRTCYC = 3) QPNRT search. The plotted points display the scatter-pattern of apparent convergence (**dbrms**) versus system size (**nbas**), with horizontal and vertical dashed/dotted lines marking overall averages for the distributions. The overall **dbrms<sub>av</sub>** (~0.05) and **dbmax<sub>av</sub>** (~0.10) values for NRTCYC = 3 are slightly higher than corresponding values when NRTCYC is allowed to run to completion (~0.04, ~0.09, respectively), but the restricted search appears to represent a reasonable compromise between exhaustiveness and practical efficiency of the search procedure. It may seem anomalous that outlier points of largest **dbrms** (> 0.1) appear at smaller **nbas** system size (< 400), but such points actually represent simpler species in which *full* NRT convergence was achieved, with the plotted value merely showing the large improvement in the final cycle.

Table S1 also includes CPU times for individual jobs and an average CPU time for the overall data set. The latter is strongly skewed by values for the most time-consuming jobs. Larger systems naturally require greater CPU time, but for example, brassinolide (1084 bf) completes in 0.8 h, whereas lanosterol (1032 bf) requires 38.3 h. Similar disparities between size and CPU time can also be seen for “average” system sizes of the data set; for example, ibuprofen (456 bf) completes in less than 3 min but trinitrotoluene (387 bf) requires 1.5 h. In general, such disparities reflect the importance differences in numbers of three-center (allylic-like) “resonance sites,” rather than **nbas** system size *per se*. Such increases in resonance complexity trend quickly toward the extreme delocalization limit in which *no* single resonance structure achieves significant “parent” status in the final NRT expansion. This important limit in which only NRT *bond orders* (but not necessarily the individual resonance weightings) achieve well-converged numerical values was essentially inaccessible in the legacy NRT implementation of pre-*NBO7* versions, but can now be treated in relatively routine manner if available system resources suffice.

For the more ordinary small-molecule (or near-NLS) cases where resonance complexity is somewhat limited by system size, the results of Table S1 exhibit the remarkable speedups of the QPNRT convex solver compared with the legacy pre-*NBO7* algorithm. About 58% of all species in Table S1 (196/338) completed in less than 1 CPU-minute, including many species that would have been hopelessly impractical (even with significant \$NRTSTR user guidance) for pre-*NBO7* NRT evaluation. The vastly improved computational efficiency of the QPNRT convex solver is also indicated by the virtually negligible percentage of associated CPU time that is generally required for even the most demanding applications throughout Table S1.

## Summary and Conclusions

Broader historical aspects of NRT development and its diverse applications are described in a recent perspective.<sup>[17]</sup> The present work focuses on the formal algorithm of the new QPNRT convex solver that underlies the vastly improved NRT implementation in current *NBO 7.0*. QPNRT also underlies the new family of “resonance-type NBOs” (RNBOs) that were recently introduced.<sup>[18]</sup> RNBOs provide semilocalized orbital imagery that accurately maps onto “curly arrow” concepts of chemical reactivity, as originally formulated by Robinson and other pioneer bonding theorists of the prequantal era.<sup>[4]</sup> The QPNRT algorithm also yields improved utility of *NBO7*-level NRT bond orders that were recently shown to provide incisive details of chemical reaction mechanisms.<sup>[19]</sup>

As described above, the composite QPNRT algorithm involves iterative cycles of two interconnected tasks: (1) the search for additional resonance bonding patterns and associated density matrix for each new pattern and (2) solution of the convex minimization problem (5) for the optimal weightings of resonance patterns under current consideration. The convex-solver task (2) follows a well-ordered path (Fig. 1) that is independent of the chosen species and consumes relatively negligible CPU time, whereas the resonance-search task (1) can grow explosively for certain species, with concomitant growth of CPU demands. Numerical results for a data set of 338 species were used to select default values of NRT keywords that appear to have leading leverage on overall execution time (particularly NRTPAR, NRTE2, and NRTCYC). The current default keyword values appear to strike a reasonable compromise for black-box studies of systems ranging from the semilocalized near-Lewis limit to highly delocalized metallic-like behavior. However, the user is encouraged to explore use of \$NRTSTR keylist input or nondefault keyword values to obtain the best compromise between lowered variational  $D(w)$  value and required CPU cost for the species under investigation.

## Supporting Information

An Excel data file (nrt\_data\_set.xlsx, “Table S1”) summarizing NRT performance details for the 338 test species, and a text file (si\_test\_set geometries.txt) with full geometrical coordinate information for each species.

## Acknowledgments

We thank Dr. John Sharley for drawing attention to recent advances in convex programming and to Prof. Stephen Boyd and colleagues for preliminary assistance in testing OSQP applicability to NRT optimizations. Support for computational facilities was provided in part by National Science Foundation Grant CHE-0840494.

**Keywords:** natural resonance theory · natural bond orbital · chemical bonding · wavefunction analysis · bond order · convex optimization

How to cite this article: E. D. Glendening, S. J. Wright, F. Weinhold. *J. Comput. Chem.* **2019**, *40*, 2028–2035. DOI: 10.1002/jcc.25855



Additional Supporting Information may be found in the online version of this article.

- [1] (a) E. D. Glendening, F. Weinhold, *J. Comput. Chem.* **1998**, *19*, 593. (b) E. D. Glendening, F. Weinhold, *J. Comput. Chem.* **1998**, *19*, 610. (c) E. D. Glendening, J. K. Badenhoop, F. Weinhold, *J. Comput. Chem.* **1998**, *19*, 628.
- [2] (a) Z. Dong, C. R. W. Reinhold, M. Schmidtman, T. A. Müller, *J. Am. Chem. Soc.* **2017**, *139*, 7117. (b) K. V. Murphy, W. J. Morgan, Z. Sun, H. F. Schaefer, J. Agarwal, *J. Phys. Chem. A* **2017**, *121*, 998. (c) M. C. Neary, G. Parkin, *Inorg. Chem.* **2017**, *56*, 1511. (d) O. A. Gapurenko, V. Y. Lee, R. M. Minuaev, V. I. Minkin, A. Sekiguchi, *Tetrahed. Lett.* **2017**, *58*, 2054. (e) A. Rosas-Sanchez, I. Alvarado-Beltran, A. Baceiredo, D. Hashizume, N. Saffon-Merceron, V. Branchadell, T. Kato, *Angew. Chem. Int. Ed.* **2017**, *129*, 489.
- [3] P.-O. Löwdin, *Phys. Rev.* **1955**, *97*, 1474.
- [4] (a) W. O. Kermak, R. Robinson, *J. Chem. Soc.* **1922**, *121*, 427. (b) T. M. Lowry, *J. Chem. Soc.* **1923**, *1923*, 822. (c) J. Allan, A. F. Oxford, R. Robinson, J. C. Smith, *J. Chem. Soc.* **1926**, *1926*, 401. (d) C. K. Ingold, E. H. Ingold, *J. Chem. Soc.* **1926**, *1926*, 1310. (e) C. K. Ingold, *Nature* **1934**, *133*, 946. (f) C. K. Ingold, *Chem. Rev.* **1934**, *15*, 225. (g) M. D. Saltzman, *J. Chem. Educ.* **1980**, *57*, 484.
- [5] L. Pauling, G. W. Wheland, *J. Chem. Phys.* **1933**, *1*, 362. L. Pauling, *Proc. Roy. Soc. Lond. A* **1977**, *356*, 433.
- [6] F. Weinhold, *J. Chem. Educ.* **1999**, *76*, 1141.
- [7] (a) G. W. Wheland, *The Theory of Resonance and Its Applications to Organic Chemistry*, Wiley, New York, **1947**. (b) I. K. Syrkin, M. W. Diatkina, *The Structure of Molecules and the Chemical Bond*, Dover, New York, **1950**. (c) L. Pauling, *The Nature of the Chemical Bond*, 3rd ed., Cornell U. Press, Ithaca, NY, **1960**.
- [8] J. B. Foresman, Æ. Frisch, *Exploring Chemistry with Electronic Structure Methods*, 3rd ed., Gaussian, Inc., Wallingford, CT, **2015**.
- [9] K. F. Freed, *Chem. Phys. Lett.* **1968**, *2*, 255.
- [10] E. D. Glendening, J. K. Badenhoop, A. E. Reed, J. E. Carpenter, J. A. Bohmann, C. M. Morales, C. R. Landis, F. Weinhold, *NBO 6.0*, Theoretical Chemistry Institute, University of Wisconsin, Madison, **2013**.
- [11] F. Weinhold, E. D. Glendening, *NBO 6.0 Program Manual*, Theoretical Chemistry Institute, University of Wisconsin–Madison, **2013**, p. B-85ff.
- [12] E. D. Glendening, J. K. Badenhoop, A. E. Reed, J. E. Carpenter, J. A. Bohmann, C. M. Morales, P. Karafiloglou, C. R. Landis, F. Weinhold, *NBO 7.0*, Theoretical Chemistry Institute, University of Wisconsin, Madison, **2018**.
- [13] J. Nocedal, S. J. Wright, *Numerical Optimization*, 2nd ed., Springer, New York, **2006** Sec. 16.3.
- [14] (a) C. A. Coulson, *Proc. R. Soc. Lond. A* **1939**, *169*, 413. (b) C. A. Coulson, *Proc. R. Soc. Lond. A* **1951**, *207*, 91. (c) P. C. Mishra, D. K. Rai, *Mol. Phys.* **1972**, *23*, 631.
- [15] (a) H. S. Johnston, *Adv. Chem. Phys.* **1960**, *3*, 131. (b) R. A. W. Johnstone, R. M. S. Loureiro, M. Lurdes, S. Cristiano, G. Labat, *ARKIVOC* **2010**, *2010*, 142.
- [16] (a) R. M. Badger, *J. Chem. Phys.* **1934**, *2*, 128. (b) J. Cioslowski, G. Liu, R. A. M. Castro, *Chem. Phys. Lett.* **2000**, *331*, 497.
- [17] E. D. Glendening, C. R. Landis, F. Weinhold, *J. Am. Chem. Soc.* **2019**, *141*, 4156. <https://doi.org/10.1021/jacs.8b12336>.
- [18] E. D. Glendening, F. Weinhold, *J. Chem. Theor. Comput.* <https://doi.org/10.1021/acs.jctc.8b00948>.
- [19] E. D. Glendening, F. Weinhold, *Tetrahedron* **2018**, *74*, 4799.

Received: 25 March 2019

Revised: 15 April 2019

Accepted: 24 April 2019

Published online on 11 May 2019